Available online at www.sciencedirect.com
SCIENCE DIRECT®
Surface Science 573 (2004) 413–425
SURFACE SCIENCE
www.elsevier.com/locate/susc

Adsorption and reaction of bicyclic hydrocarbons at Pt(1 1 1) and Sn/Pt(1 1 1) surface alloys: *trans*-decahydronaphthalene ($C_{10}H_{18}$) and bicyclohexane ($C_{12}H_{22}$)

Haibo Zhao, Bruce E. Koel *

Department of Chemistry, University of Southern California, SSC 606, Los Angeles, CA 90089-0482, USA

Received 6 July 2004; accepted for publication 7 October 2004
Available online 22 October 2004

Abstract

Adsorption and desorption of *trans*-decahydronaphthalene ($C_{10}H_{18}$) and bicyclohexane ($C_{12}H_{22}$) can be used to probe important aspects of non-specific dehydrogenation leading to surface carbon accumulation and establish better estimates of activation energies for C–H bond cleavage at Pt–Sn alloys. This chemistry was studied on Pt(1 1 1) and the (2×2)-Sn/Pt(1 1 1) and $(\sqrt{3}\times\sqrt{3})R30°$-Sn/Pt(1 1 1) surface alloys by using temperature programmed desorption (TPD) mass spectroscopy and Auger electron spectroscopy (AES). These hydrocarbons are reactive on Pt(1 1 1) surfaces and fully dehydrogenate at low coverages to produce H_2 and surface carbon during TPD. At monolayer coverage, 87% of adsorbed $C_{10}H_{18}$ and 75% $C_{12}H_{22}$ on Pt(1 1 1) desorb with activation energies of 70 and 75 kJ/mol, respectively. Decomposition of $C_{10}H_{18}$ is totally inhibited during TPD on these Sn/Pt(1 1 1) alloys and decomposition of $C_{12}H_{22}$ is reduced to 10% of the monolayer coverage on the (2×2)-Sn/Pt(1 1 1) alloy and totally inhibited on the $(\sqrt{3}\times\sqrt{3})R30°$-Sn/Pt(1 1 1) alloy. $C_{10}H_{18}$ and $C_{12}H_{22}$ are more weakly chemsorbed on these two alloys compared to Pt(1 1 1) and these molecules desorb in narrow peaks characteristic of each surface with activation energies of 65 and 73 kJ/mol on the (2×2) alloy and 60 and 70 kJ/mol on the $(\sqrt{3}\times\sqrt{3})R30°$-Sn/Pt(1 1 1) alloy, respectively. Alloyed Sn has little influence on the monolayer saturation coverage of these two molecules, and this is decreased only slightly on these two Sn/Pt(1 1 1) alloys. The use of these two probe molecules enables an improved estimate of the activation energy barriers E^* to break aliphatic C–H bonds in alkanes on Sn/Pt alloys; $E^* = 65$–73 kJ/mol on the (2×2)-Sn/Pt(1 1 1) alloy and $E^* \geqslant 70$ kJ/mol on the $(\sqrt{3}\times\sqrt{3})R30°$-Sn/Pt(1 1 1) alloy.

Keywords: Alloys; Platinum; Tin; Alkanes; Thermal desorption; Auger electron spectroscopy; Catalysis

* Corresponding author. Tel.: +1 213 740 4126; fax: +1 213 740 3972.
E-mail address: koel@usc.edu (B.E. Koel).

0039-6028/$ - see front matter © 2004 Elsevier B.V. All rights reserved.
doi:10.1016/j.susc.2004.10.009

1. Introduction

Bimetallic Pt–Sn catalysts are commercially important for suppressing the hydrogenolysis that can occur on pure-Pt catalysts [1,2]. Practical economic issues and superior performance at low pressures makes alumina-supported Pt–Sn catalysts an important commercial system in naphtha reforming [3]. In addition, Pt–Sn catalysts are promising systems for efficient reforming that is needed for hydrocarbon fuel cells and are known to catalyze a variety of selective dehydrogenation and hydrogenation reactions. For example, Cortright and Dumesic have reported a highly active and selective Pt/Sn/K–L zeolite catalyst for isobutene dehydrogenation in which Pt–Sn alloy particles are formed [4–6]. Recent developments by Schmidt and coworkers [7–9] have shown that thick metal films used in millisecond-partial oxidation reactions may be useful in natural gas oxidation to produce CO and H_2 and direct oxidation of ethane to ethylene. For example, thick Pt–Sn alloy films on alumina monoliths have shown high selectivities (85%) and activities (70% conversion) for direct oxidation of ethane to ethylene. The surface remains almost clean after these reactions.

Addition of tin in reforming catalysts plays an important role in selectivity and catalyst lifetimes [10]. Sn is considered to reduce C–H and C–C bond breaking activity of Pt catalysts in hydrocarbon reforming reactions, and this influence presumably extends to these newer applications as well. Specifically, Pt–Sn alloy phases are relevant to the action of many of these catalysts and alloyed Sn has been shown to strongly decrease the reactivity of many hydrocarbons and organic molecules on Pt(1 1 1) surfaces in surface science studies under UHV conditions [11–20].

A quantitative elucidation of hydrocarbon thermochemistry on these Pt–Sn alloys remains an elusive goal to better understand catalytic reaction mechanisms on these catalysts. Such diagrams exist for Pt(1 1 1) [21,22]. However, on Pt–Sn alloys, the value for the activation energy barrier to C–H bond cleavage in alkanes, alkenes, and other hydrocarbons remains a key fundamental question. This problem arises in part because alkanes (saturated hydrocarbons) interact weakly when molecularly adsorbed on low-Miller index Pt surfaces, and even more weakly on Pt–Sn alloys. Thus, small saturated hydrocarbons have low desorption activation energies and desorb at low temperatures, which leads to reversible adsorption of these molecules under UHV conditions, i.e., no decomposition occurs. For example, butane and isobutane adsorb reversibly on two Sn/Pt(1 1 1) alloy surfaces with desorption energies below 40 kJ/mol [11]. C_5–C_8 cycloalkanes are all reversibly adsorbed on two Sn/Pt(1 1 1) alloy surfaces (a trace amount of dehydrogenation was observed on the (2×2)Sn/Pt(1 1 1) surface, possibly due to defects) [12,13]. Currently, these desorption activation energies (40–58 kJ/mol) can be used to place a lower limit on the activation energy barrier E^* to break primary C–H bonds in alkanes and cycloalkanes on Sn/Pt alloys. However, these numbers are likely to be much too small. In order to determine the value of E^*, or at least place a more realistic bound on it, we need to use larger, more strongly adsorbed hydrocarbon molecules that will remain adsorbed at the alloy surface until temperatures are reached where decomposition occurs.

trans-Decahydronaphthalene ($C_{10}H_{18}$) and bicyclohexane ($C_{12}H_{22}$) are shown in Scheme 1. Both molecules are comprised of two rings and should interact significantly stronger with the surface than those molecules mentioned above. This gives us a better chance to observe C–H bond dissociation due to the increased desorption activation energy. $C_{10}H_{18}$ and $C_{12}H_{22}$ are of interest in their own right, because they are components of a series of diesel and jet fuel blends made from catalytic reforming processes [23]. However, there have been no previous surface science studies reported for $C_{10}H_{18}$ and $C_{12}H_{22}$ adsorption on metal surfaces. Surface science studies of adsorption and

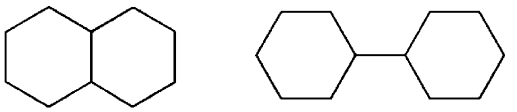

Scheme 1.

desorption of these molecules on Pt and Pt–Sn alloys provides basic information that is helpful in understanding catalytic reforming processes.

In the present study, we investigated the interaction of $C_{10}H_{18}$ and $C_{12}H_{22}$ with Pt(1 1 1) and two Sn/Pt(1 1 1) alloys under UHV conditions by temperature-programmed desorption (TPD) and Auger electron spectroscopy (AES). We used two, well-defined, ordered, Pt–Sn surface alloys denoted as the (2×2)Sn/Pt(1 1 1) and $(\sqrt{3}\times\sqrt{3})R30°$-Sn/Pt(1 1 1) alloys prepared by evaporating Sn onto a Pt(1 1 1) surface and annealing the sample to 1000 K, as first reported by Paffett and Windham [24]. Subsequently, these surfaces have been extensively characterized by LEISS [25], LEED I–V [26], XRD [27], and STM [28,29]. These Sn/Pt(1 1 1) surface alloys offer outstanding new opportunities for fundamental surface science and catalytic study at the molecular level.

2. Experimental methods

Experiments were performed in a three-level UHV chamber as described earlier [30]. The Pt(1 1 1) crystal (Atomergic; 10-mm dia., 1.5-mm thick) was prepared by using 1-keV Ar^+-ion sputtering and oxygen exposures (5×10^{-7}-Torr O_2, at 900 K for 2 min) to give a clean spectrum using Auger electron spectroscopy (AES) and a sharp (1×1) pattern in low energy electron diffraction (LEED).

The (2×2)-Sn/Pt(1 1 1) and $(\sqrt{3}\times\sqrt{3})R30°$-Sn/Pt(1 1 1) surface alloys, as shown in Scheme 2, were prepared by evaporating two monolayers of Sn onto the Pt(1 1 1) crystal surface and subsequently annealing the sample for 20 s to 1000 and 830 K, respectively. Sn is incorporated substitutionally into primarily only the surface layer to form an ordered alloy or intermetallic compound with $\theta_{Sn} = 0.25$ on the (2×2)-Sn/Pt(1 1 1) alloy, with a composition corresponding to the (1 1 1) face of a bulk Pt_3Sn crystal, and $\theta_{Sn} = 0.33$ on the $(\sqrt{3}\times\sqrt{3})R30°$-Sn/Pt(1 1 1) alloy, with a composition corresponding to a Pt_2 Sn surface. These surface alloys are relatively "flat", but Sn atoms protrude 0.02 nm above the surface-Pt plane at both surfaces [25]. In the (2×2) structure, pure-

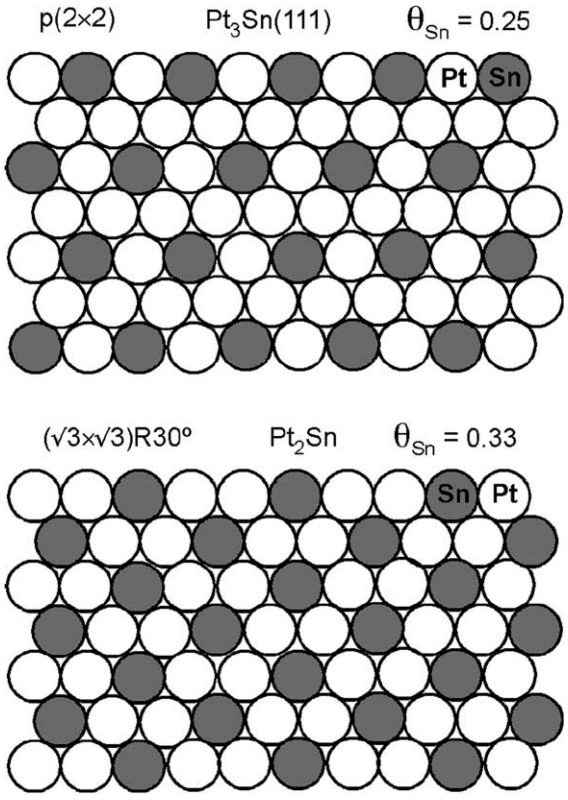

Scheme 2.

Pt three-fold reactive sites are present, but no adjacent pure-Pt three-fold sites exist. All pure-Pt three-fold sites are eliminated in the $(\sqrt{3}\times\sqrt{3})R30°$ structure, and only two-fold pure-Pt sites are present. For brevity throughout this paper, we will refer to the $p(2\times2)$-Sn/Pt(1 1 1) and $(\sqrt{3}\times\sqrt{3})R30°$-Sn/Pt(1 1 1) surface alloys as the (2×2) and $\sqrt{3}$ alloys, respectively.

trans-Decahydronaphthalene ($C_{10}H_{18}$, Aldrich Chem. Co., 99%) and bicyclohexane ($C_{12}H_{22}$, Aldrich Chem. Co., 99%) were placed in a glass reservoir attached to a stainless-steel dosing line and used as supplied after degassing by multiple freeze-pump-thaw cycles. The gases were exposed on the Pt crystal by a microcapillary array doser connected to the gas line through a variable leak valve. All of the exposures reported here are given simply in terms of the background pressure in the UHV chamber as measured by an ion gauge. No

attempt was made to correct for the flux enhancement of the doser or ion gage sensitivity. The mass spectrometer in the chamber was used to check the purity of the gases during dosing.

For all TPD experiments, the heating rate was 3.6 K/s and all exposures were given with the surface temperature at 110 K or below. AES measurements were made with a double-pass cylindrical mirror analyzer (CMA) using a modulation voltage of 4 eV. The electron gun was operated at 3-keV beam energy and 1.5-μA beam current.

3. Results

3.1. trans-Decahydronaphthalene ($C_{10}H_{18}$)

Possible decomposition products produced during TPD following adsorption of *trans*-decahydronaphthalene ($C_{10}H_{18}$) were examined by monitoring 24 signals, including those at 138, 136, 134, 132, 130, 128, 78, 80, 82, 67, and 2 amu. Based on analysis of the shape and peak temperature of all of these signals during TPD, only the desorption of H_2 and the parent molecule, $C_{10}H_{18}$, were detected from all three surfaces studied. A series of TPD spectra for $C_{10}H_{18}$ desorption after $C_{10}H_{18}$ adsorption on Pt(1 1 1) at 110 K is shown in Fig. 1. The signal at 67 amu is due to the primary cracking peak from $C_{10}H_{18}$ and was used to monitor $C_{10}H_{18}$ desorption. A clear separation occurs between a high-temperature peak at 275 K due to a chemisorbed state and a low-temperature peak at 199 K arising from desorption from a physisorbed layer. Increasing the coverage further causes a new peak at 189 K to appear. The peak at 199 K eventually saturates in intensity with increasing exposure, but the peak at 189 K does not. We assign the peaks at 199 and 189 K as due to desorption of second-layer and multilayer species, respectively.

H_2 evolution, as shown in Fig. 2, monitors complete $C_{10}H_{18}$ decomposition on Pt(1 1 1). The amount of H_2 desorption saturates after 0.3-L $C_{10}H_{18}$ exposure, prior to reaching monolayer coverage. Five H_2 desorption peaks can be identified at 288, 318, 466, 516, and 602 K, which indicates that several elementary steps are needed to complete the decomposition process. The total amount of H_2 evolved in TPD after large exposures of $C_{10}H_{18}$ is 0.20 ML H_2, correspond to the complete decomposition of 0.0224-ML $C_{10}H_{18}$. The amount of H_2 was determined by comparison of this H_2 TPD peak area to a reference H_2 TPD spectrum obtained after ethylene (C_2H_4) exposures on Pt(1 1 1) at 300 K to produce 0.25-ML ethylidyne (CCH_3) [31], in which complete decomposition produces 0.375-ML H_2, i.e. $\theta_H = 0.75$ ML. This value was also checked by comparison to a reference H_2 TPD spectrum obtained after a 300-L H_2 exposure on Pt(1 1 1) at 110 K, in which θ_H was reported to be 0.8 ML [32]. The amount of H_2 obtained by using the second method was 10% higher than that obtained by using the first method.

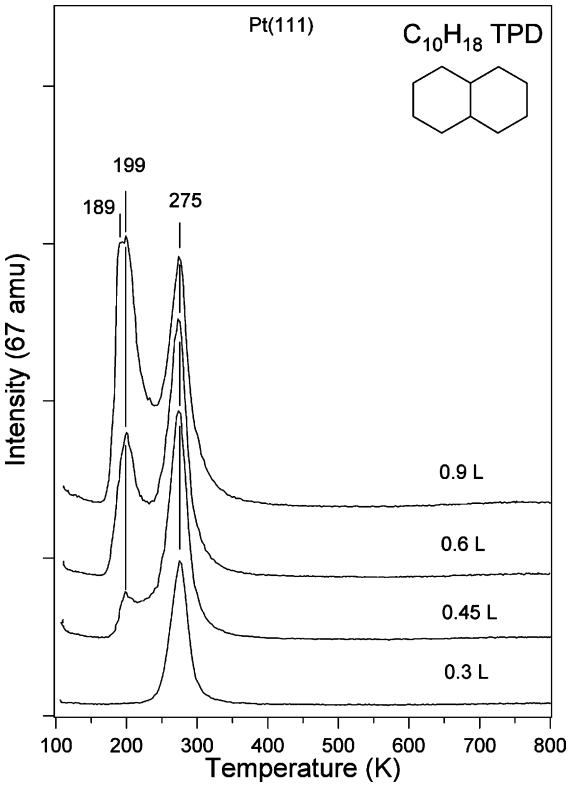

Fig. 1. $C_{10}H_{18}$ TPD spectra after *trans*-decahydronaphthalene ($C_{10}H_{18}$) exposures on Pt(1 1 1) at 110 K.

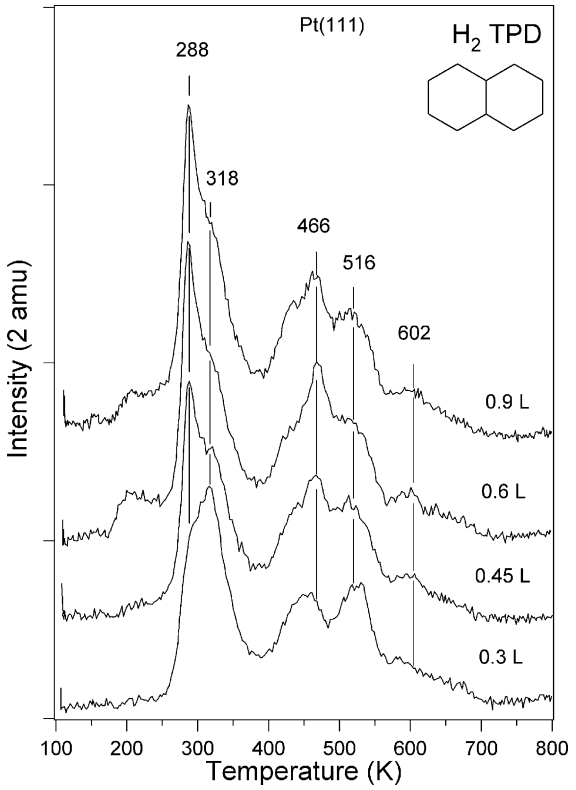

Fig. 2. H_2 TPD spectra after *trans*-decahydronaphthalene ($C_{10}H_{18}$) exposures on Pt(1 1 1) at 110 K.

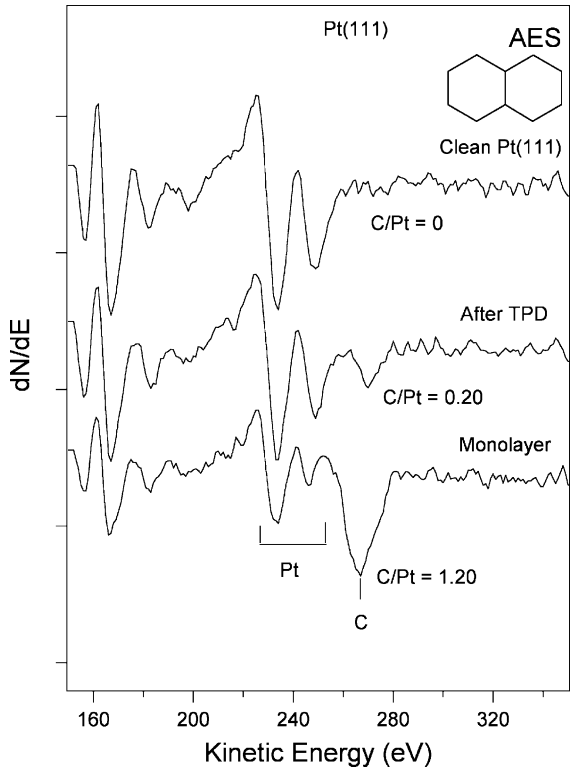

Fig. 3. AES spectra of clean Pt(1 1 1) (top), monolayer $C_{10}H_{18}$-covered Pt(1 1 1) (bottom), and the Pt(1 1 1) surface following a 0.6-L $C_{10}H_{18}$ TPD experiment (middle).

The C (272 eV)/Pt (237 eV) peak-to-peak ratio in AES was used to determine the monolayer coverage of $C_{10}H_{18}$ on Pt(1 1 1) and the amount of residual carbon left on the surface following heating to 800 K in TPD, as shown in Fig. 3. The AES spectrum for the $C_{10}H_{18}$ monolayer was taken after dosing 0.45-L $C_{10}H_{18}$ on Pt(1 1 1) at 110 K and annealing at 210 K for 5 s. The amount of carbon present on the surface decreased after TPD due to desorption of reversibly adsorbed $C_{10}H_{18}$. We can estimate the amount of surface carbon from an AES calibration using 0.25-ML ethylidyne (CCH_3) on Pt(1 1 1) at 300 K [31], which corresponds to $\theta_C = 0.5$ ML and gives C(272)/Pt(237) = 0.35. We find that $\theta_C = 1.71$ ML and $\theta_{C_{10}H_{18}} = 0.17$ ML in the $C_{10}H_{18}$ monolayer and $\theta_C = 0.29$ ML was left on the surface following TPD. This corresponds to the complete decomposition of $\theta^{dec}_{C_{10}H_{18}} = 0.029$ ML or 16.8% of the amount of $C_{10}H_{18}$ monolayer. This is consistent with the extent of decomposition calculated independently by using the H_2 TPD area, which gives $\theta^{dec}_{C_{10}H_{18}} = 0.0224$ ML corresponding to 13.1% decomposition.

A similar series of TPD spectra for $C_{10}H_{18}$ desorption from the (2×2) and $\sqrt{3}$ alloys are shown in Figs. 4 and 5, respectively. In each case, a high-temperature desorption peak was assigned to desorption from a chemisorbed state and low-temperature desorption peaks was assigned to desorption from physisorbed states. No distinct peak from desorption of second-layer molecules was observed between the monolayer and multilayer features. Physisorbed molecules in the condensed phase, multilayer desorb in a peak at 186 K on both of these two alloys after large

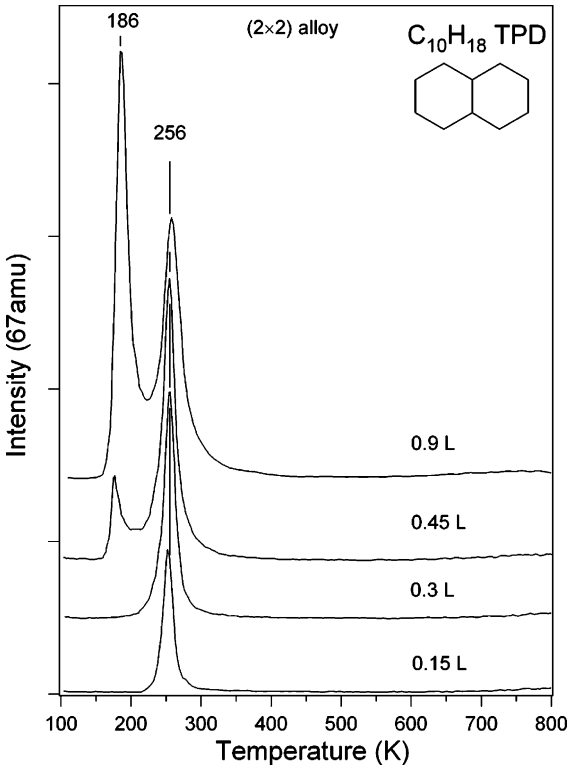

Fig. 4. $C_{10}H_{18}$ TPD spectra after *trans*-decahydronaphthalene ($C_{10}H_{18}$) exposures on a (2×2)Sn/Pt(1 1 1) surface alloy at 110 K.

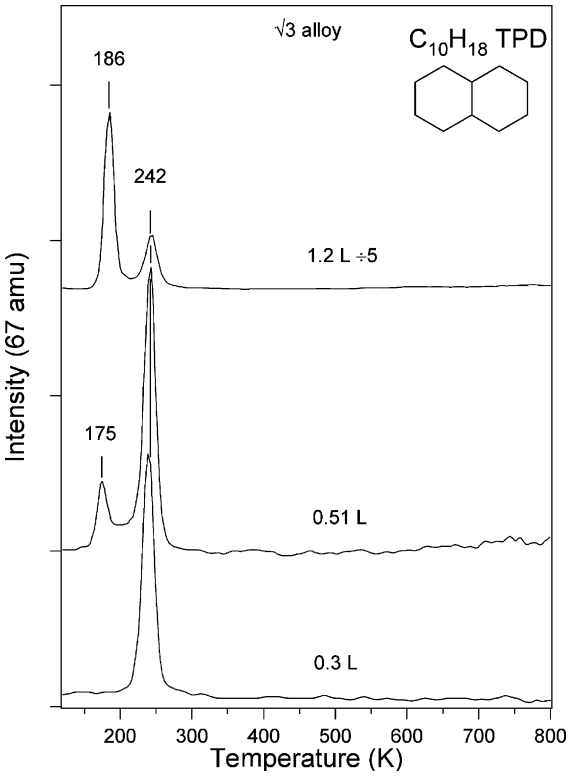

Fig. 5. $C_{10}H_{18}$ TPD spectra after *trans*-decahydronaphthalene ($C_{10}H_{18}$) exposures on a $(\sqrt{3}\times\sqrt{3})R30°$-Sn/Pt(1 1 1) surface alloy at 110 K.

exposures. Desorption from the monolayer appeared at 256 K on the (2×2) alloy and 242 K on the $\sqrt{3}$ alloy. The peak shapes and absence of a shift with increasing $C_{10}H_{18}$ coverage on both of these surface alloys and on Pt(1 1 1) indicate first-order desorption kinetics.

Assuming first-order desorption kinetics with a preexponential factor of $10^{13}\,s^{-1}$, the Redhead method [33] gives an estimate of the desorption activation energy E_d of 70, 65, 60 kJ/mol for $C_{10}H_{18}$ adsorbed in the monolayer on Pt(1 1 1) and the (2×2) and $\sqrt{3}$ alloys, respectively.

No appreciable amount of H_2 was detected during TPD from the two Pt–Sn alloys following $C_{10}H_{18}$ exposures and no carbon was detected by AES following TPD. Thus, $C_{10}H_{18}$ is completely reversibly adsorbed on these two alloys under these conditions and no decomposition occurs during TPD.

3.2. Bicyclohexane ($C_{12}H_{22}$)

$C_{12}H_{12}$ and H_2 were the only two desorption products detected in TPD following $C_{12}H_{12}$ exposures on Pt(1 1 1) at 110 K. The signal at 82 amu is the major cracking peak of $C_{12}H_{12}$ and was used to monitor the desorption of $C_{12}H_{12}$. TPD spectra for $C_{12}H_{22}$ desorption from Pt(1 1 1) are shown in Fig. 6. After exposures less than 0.4 L, no $C_{12}H_{12}$ desorption was detected during heating in TPD. When the coverage was increased after larger exposures, a single peak at 291 K was observed initially due to desorption from a chemisorbed state and then a low-temperature peak at 210 K arose from desorption from a condensed, physisorbed layer. No clearly resolved $C_{12}H_{12}$ desorption peak from second-layer physisorbed species was observed.

H_2 evolution from $C_{12}H_{22}$ decomposition on Pt(1 1 1) during TPD is shown in Fig. 7. For

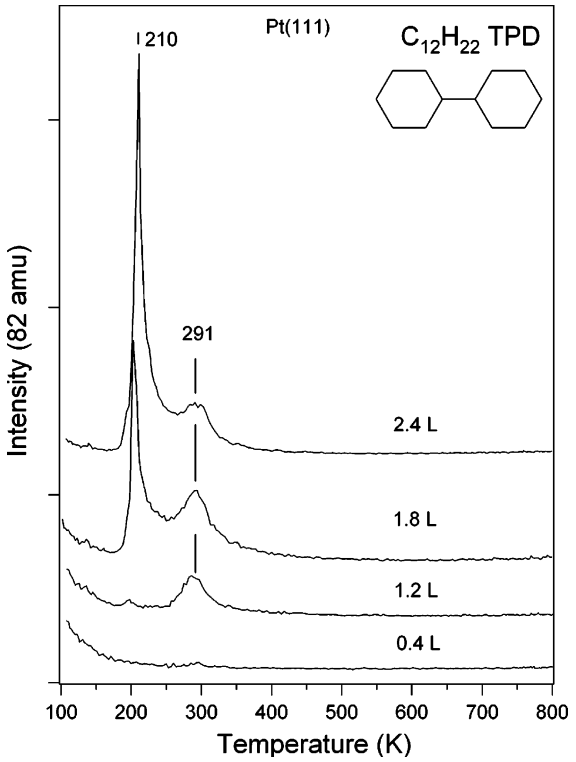

Fig. 6. $C_{12}H_{22}$ TPD spectra after bicyclohexane ($C_{12}H_{22}$) exposures on Pt(111) at 110 K.

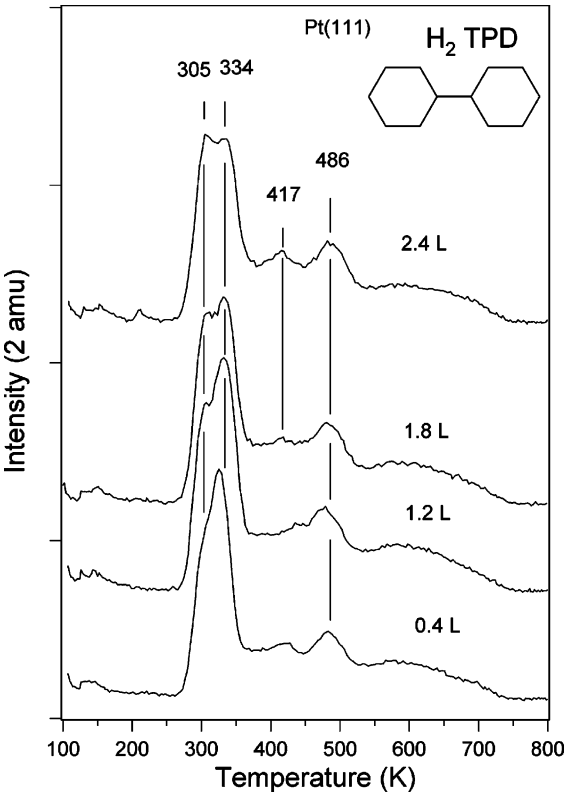

Fig. 7. H_2 TPD spectra after bicyclohexane ($C_{12}H_{22}$) exposures on Pt(111) at 110 K.

increasing $C_{12}H_{22}$ exposures, the amount of H_2 desorption increased until after a 1.2-L $C_{12}H_{22}$ exposure. Four desorption features can be identified at 305, 334, 417, and 486 K corresponding to sequential decomposition steps. The maximum yield in the H_2 TPD curves from $C_{12}H_{22}$ exposures in Fig. 7 corresponds to $\theta_H = 0.89$ ML. Using an ethylidyne Ref. [31], this indicates that 0.040-ML $C_{12}H_{22}$ decomposed during heating in TPD.

Fig. 8 shows AES spectra from Pt(111) after $C_{12}H_{22}$ experiments. A $C_{12}H_{22}$ monolayer was obtained by dosing 1.2-L $C_{12}H_{22}$ on Pt(111) at 110 K and then annealing to 220 K for 5 s. By using the C(272)/Pt(237) AES peak ratio from ethylidyne [31], we determined that $\theta_C = 1.92$ ML, or $\theta_{C_{12}H_{22}} = 0.16$ ML in the monolayer, and $\theta_C = 0.60$ ML left on the surface following TPD. This corresponds to $\theta^{dec}_{C_{12}H_{11}} = 0.050$ ML, or 31% of the $C_{12}H_{22}$ monolayer. This is fairly consistent with the value of 25% of the $C_{12}H_{22}$ monolayer that decomposed deduced from the H_2 TPD measurements in Fig. 7.

On the (2×2) surface alloy, some irreversible $C_{12}H_{12}$ adsorption occurred during TPD experiments, but no desorption products other than $C_{12}H_{12}$ and H_2 were detected. Fig. 9 shows TPD spectra for $C_{12}H_{12}$ desorption following $C_{12}H_{12}$ dosing on the (2×2) surface alloy at 110 K. The peak maximum for desorption from the chemisorbed monolayer occurs at 286 K. This value varies only slightly with changes in the coverage. A desorption peak at 206 K, the same temperature as that observed on Pt(111), forms after large exposures due to desorption of physisorbed species.

H_2 TPD spectra shown in Fig. 10 were used to monitor $C_{12}H_{22}$ decomposition on the (2×2) alloy. The H_2 desorption yield saturated after a 1.35-L $C_{12}H_{22}$ exposure. H_2 desorption initially

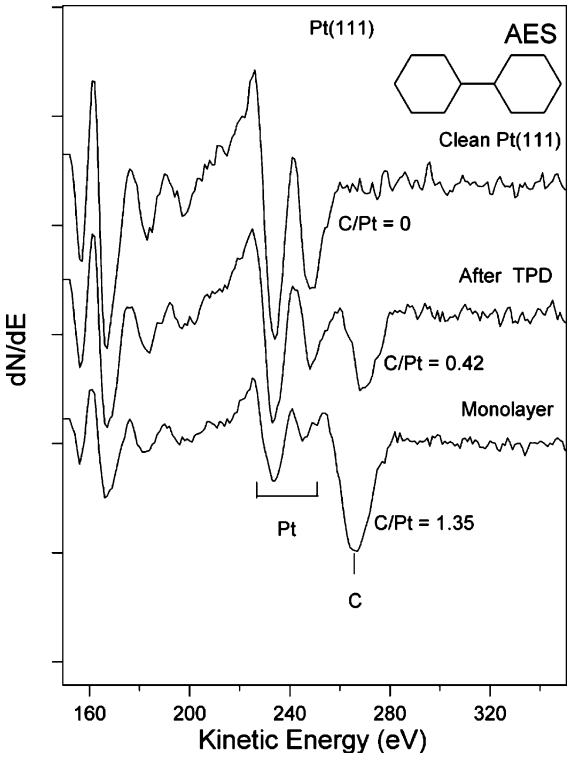

Fig. 8. AES spectra of clean Pt(1 1 1) (top), monolayer $C_{12}H_{22}$-covered Pt(1 1 1) (bottom), and the Pt(1 1 1) surface following a 1.2-L $C_{12}H_{22}$ TPD experiment (middle).

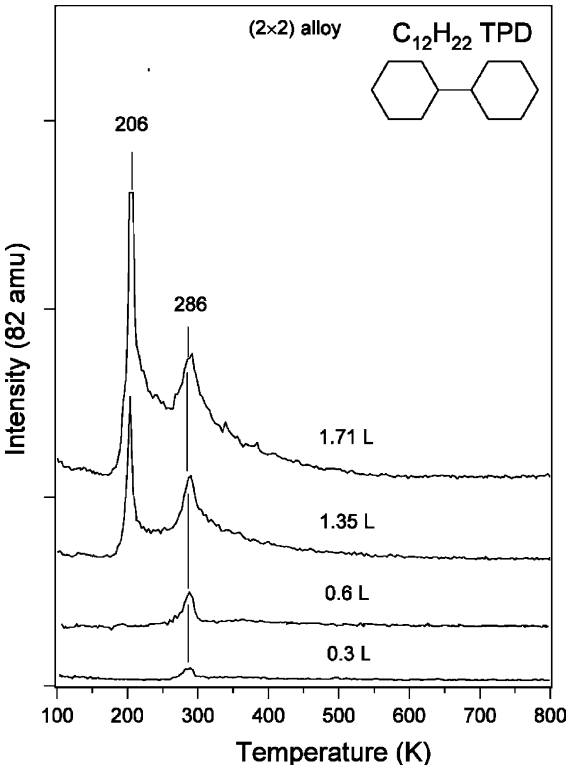

Fig. 9. $C_{12}H_{22}$ TPD spectra after bicyclohexane ($C_{12}H_{22}$) exposures on a (2×2)Sn/Pt(1 1 1) surface alloy at 110 K.

had a feature near 291 K and a broad peak evolved near 370 K with increasing exposures. The maximum amount of H_2 evolved in Fig. 10 corresponds to $\theta_H = 0.35$ ML, using the same ethylidyne reference as before, which indicates that $\theta^{dec}_{C_{12}H_{22}} = 0.016$ ML. The amount of $C_{12}H_{22}$ that was desorbed in TPD was $\theta = 0.145$ ML, as determined by comparison to the $C_{12}H_{22}$ TPD area and amount of $C_{12}H_{22}$ desorbed from Pt(1 1 1), and so the monolayer coverage of 0.161 ML could be obtained by adding the amount of $C_{12}H_{22}$ desorbed and decomposed. This amount is almost same as that on Pt(1 1 1). About 10% of the $C_{12}H_{22}$ monolayer on the (2×2) alloy decomposed during heating in TPD.

$C_{12}H_{22}$ reversibly adsorbs and desorbs molecularly from the $\sqrt{3}$ alloy without any decomposition. This was deduced by the absence of any detectable signal at 2 amu in TPD due to H_2 desorption and by the lack of any carbon signal in AES following TPD. A series of TPD spectra obtained at 82 amu for $C_{12}H_{22}$ desorption from the $\sqrt{3}$ alloy are shown in Fig. 11. Desorption of $C_{12}H_{12}$ from the monolayer on this alloy occurs in a peak at 275 K that does not shift significantly with increasing coverage. Desorption from physisorbed species produced after large exposures occurs in a peak at 206 K, which is same as that on the (2×2) alloy and close to that on Pt(1 1 1).

Redhead analysis using the $C_{12}H_{22}$ desorption peak maxima of TPD peaks at moderate coverages in the chemisorbed monolayer on the three surfaces provides desorption activation energies of 75, 73, and 70 kJ/mol on Pt(1 1 1) and the (2×2) and $\sqrt{3}$ alloys, respectively.

Fig. 12 summarizes the influence of alloyed Sn on the monolayer coverage, desorption activation energy, and amount of decomposition of these

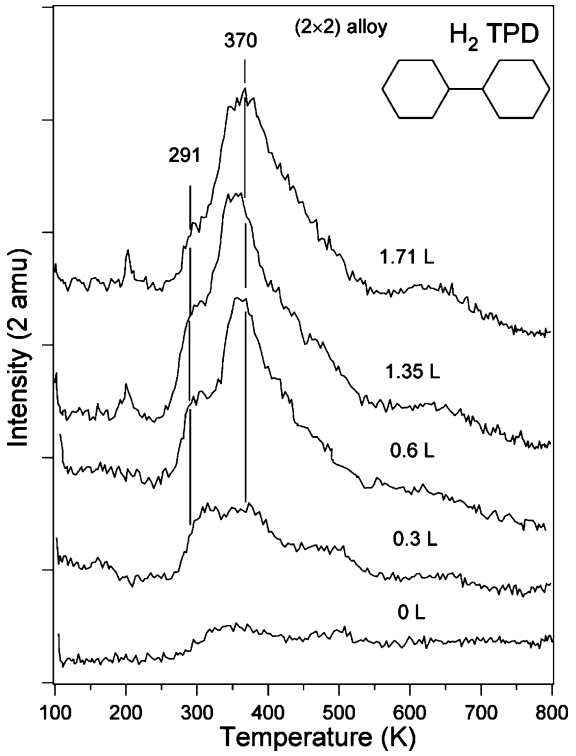

Fig. 10. H_2 TPD spectra after bicyclohexane ($C_{12}H_{22}$) exposures on a (2×2)Sn/Pt(1 1 1) surface alloy at 110 K.

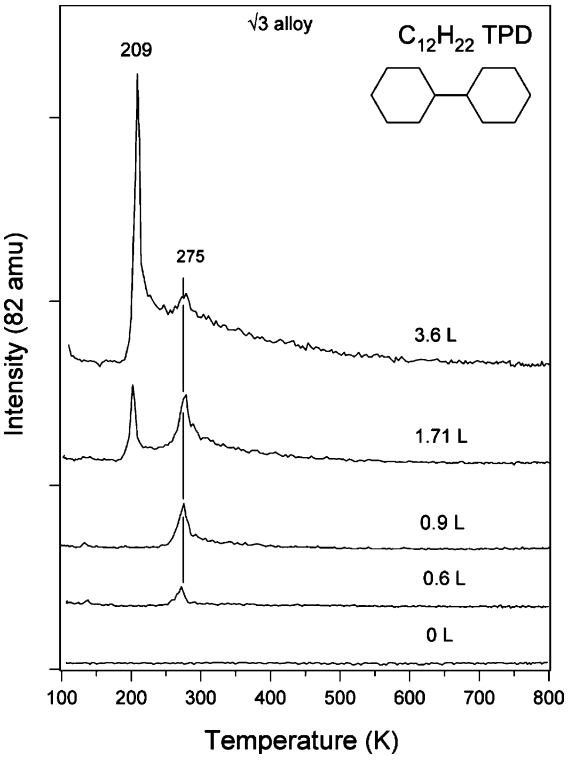

Fig. 11. $C_{12}H_{22}$ TPD spectra after bicyclohexane ($C_{12}H_{22}$) exposures on a $(\sqrt{3}\times\sqrt{3})R30°$-Sn/Pt(1 1 1) surface alloy at 110 K.

two closely related molecules. The coverage in the chemisorbed monolayer and the amount of decomposition are given on the left-hand scale of Fig. 12. The saturation coverage of chemisorbed $C_{10}H_{18}$ and $C_{12}H_{22}$ are nearly the same on each surface, and the coverage of each molecule slightly decreases only slightly with increasing Sn concentration in the alloys. However, the reactivity of the alloy surfaces, as probed by the decomposition of both molecules, decreases noticeably with increasing Sn concentration. $C_{10}H_{18}$ decomposition (13% on Pt(1 1 1)) is completely inhibited on both surface alloys while $C_{12}H_{22}$ decomposition (25% on Pt(1 1 1)) decreases on the (2×2) alloy to 10% and is completely inhibited on the $\sqrt{3}$ alloy. The adsorption energy, which is equal to the desorption activation energy (E_d) in the case of non-activated adsorption (as is the case here), decreases for both molecules only slightly with increasing Sn concentration in the Sn/Pt(1 1 1) alloy surface. However, this change is non-linear, which illustrates the importance of "reactive sites" and specific surface geometries rather than a generalized scaling or homogeneous influence of θ_{Sn}.

4. Discussion

Adsorption and desorption of alkanes [11,34] and cycloalkanes [12,13] on Pt(1 1 1) and two Sn/Pt(1 1 1) alloys under UHV conditions have been studied previously, and many aspects of the influence of alloyed Sn on this chemistry can be described. Linear alkanes are reversibly adsorbed on Pt(1 1 1), up to at least *n*-hexane (C_6H_{14}), and do not decompose during heating in TPD. However, the cycloalkanes are more reactive. While *n*-hexane [34] has the same desorption activation

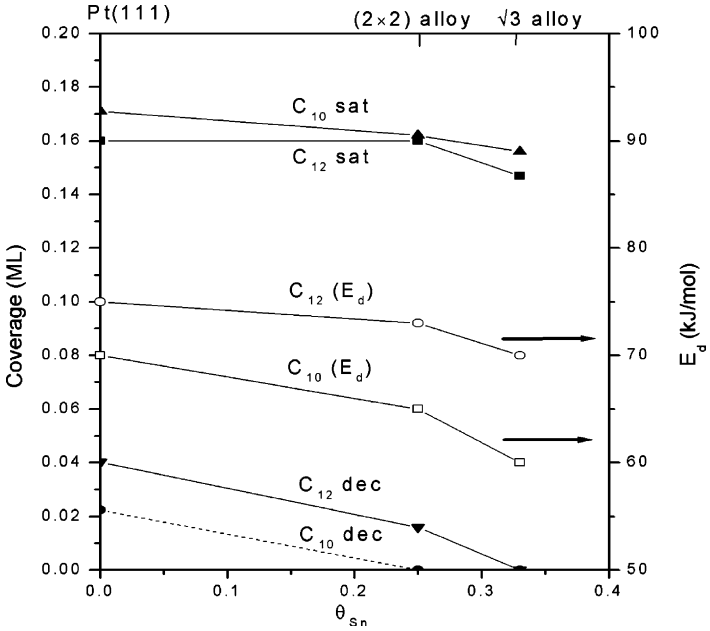

Fig. 12. Influence of alloyed Sn on $C_{10}H_{18}$ and $C_{12}H_{22}$ adsorption and reaction on Pt(111) and two Sn/Pt(111) surface alloys.

energy, E_d = 58 kJ/mol, as cyclohexane (c-C_6H_{12}) on Pt(111) [12], dehydrogenation of cyclohexane also occurs with desorption during TPD on Pt(111) [12,35]. This dehydrogenation takes place in a step-wise fashion, first to form adsorbed cyclohexyl groups with a barrier of E^* = 42 kJ/mol, eventually forming benzene [22], and then adsorbed benzene dehydrogenates further to release H_2 at higher temperature in TPD. Methylcyclohexane (c-C_7H_{14}), even though it has the same adsorption energy, E_d = 56–61 kJ/mol [36,37], as cyclohexane, contains tertiary (3°) C–H bonds that are weaker and more reactive [38]. Consistently, 45% of the adsorbed monolayer decomposes on Pt(111) during TPD [36] via a barrier that is predicted to be lower than that for cyclohexane dehydrogenation.

As expected, $C_{10}H_{18}$ (*trans*-decahydronaphthalene) and $C_{12}H_{22}$ (bicyclohexane) both decomposed on Pt(111) during TPD. Presumably $C_{10}H_{18}$ dehydrogenates step-wise by losing 10 H atoms to form adsorbed naphthalene as one eventual intermediate. Adsorbed naphthalene continues to dehydrogenate and liberate additional H_2 in TPD. This view is supported by the fact that the H_2 TPD area below 400 K and that above 400 K in Fig. 2 has a ratio close to 5:4. Similarly, adsorbed biphenyl may act as the intermediate during the dehydrogenation of $C_{12}H_{22}$ since the H_2 TPD area below 400 K and that above 400 K in Fig. 2 has a ratio close to 6:5.

Although both $C_{12}H_{22}$ and $C_{10}H_{18}$ have bicyclic ring structures, different carbon numbers and structures lead to a small difference in the adsorption energies, i.e., 75 and 70 kJ/mol, respectively. The larger adsorption energy of $C_{12}H_{22}$ leads to a higher reactivity and the percentage of $C_{12}H_{22}$ that decomposes (25%) in the monolayer on Pt(111) during TPD is almost twice that of $C_{10}H_{18}$ (13%). We expect that the C–H bond dissociation barrier on Pt(111) for these cycloalkanes, which have secondary (2°) and tertiary (3°) C–H bonds, is the same or lower than that for cyclohexane, which has only secondary (2) C–H bonds, and similar to that of methylcyclohexane. Thus, no new information is gained about the C–H bond dissociation barrier E^* on Pt(111). No information about the barrier for C–C bond scission was obtained either, because no carbon-containing decomposition products were detected in

TPD (other than the parent molecules) and no spectroscopic evidence was obtained for the surface species formed during TPD.

The replacement of 25% or more of the surface Pt atoms by Sn, $\theta_{Sn} \geqslant 0.25$, in the surface alloys suppressed $C_{10}H_{18}$ dehydrogenation completely under these conditions. This was observed previously for cyclohexane [12]. $C_{12}H_{22}$ is more strongly adsorbed and forming the $\sqrt{3}$ surface alloy with $\theta_{Sn} = 0.33$ was required to totally stop dehydrogenation during TPD. On the (2×2) alloy, the desorption energy of $C_{12}H_{22}$ (73 kJ/mol) is 8 kJ/mol higher than that of $C_{10}H_{18}$ (65 kJ/mol) and this allows dehydrogenation to compete with desorption at low coverages. Thus, we can estimate that the 3°-C–H bond dissociation barrier $E^* = 65$–73 kJ/mol on the (2×2) alloy, and $E^* > 70$ kJ/mol on the $\sqrt{3}$ alloy. This can be compared to that on Pt(1 1 1) where $E \leqslant 42$ kJ/mol.

The barrier to breaking the first C–H bond in adsorbed cycloalkanes on the $\sqrt{3}$ alloy is much higher than that to break the next C–H bond in a subsequent reaction. This assertion comes from results using surface-bound cyclohexyl species that were created on all three of these surfaces to explore dehydrogenation reactions [12]. On the $\sqrt{3}$ alloy, cyclohexene that was produced from cyclohexyl dehydrogenation desorbed at 208 K (and even this was thought to be desorption-rate-limited). Thus, C–H bond scission in cyclohexyl dehydrogenation occurs at much lower temperatures than 275 K where $C_{12}H_{22}$ desorbed molecularly without any decomposition.

An understanding of the origin of the increase in the C–H bond-breaking barrier upon alloying Pt with Sn is still forthcoming. The electronic structure of the two Sn/Pt(1 1 1) surface alloys studied here was characterized previously by using UPS [39] and XPS [40]. XPS showed no significant chemical shifts of the Pt core level peaks, and only small changes occurred in the UPS spectra upon alloying. However, UPS spectra of the alloys were not a simple addition of Pt and Sn spectra, and some new features were attributed to either a strongly modified band of a single component or some kind of common band of Sn and Pt. Electronic structure calculations of bulk Pt_3Sn alloys by Pick [41] showed that bonding interactions between Pt and Sn in the alloy changed the local electronic structure at Pt and Sn sites. Hybridization between Pt-d and Sn-p electrons leads to a lowering of the LDOS at the Fermi level and a downward shift of the Pt local d-band. Depopulation of the Pt 5d-band, and the loss of adjacent pure-Pt 3-fold hollow sites, in the (2×2) alloy evidently lead to the formation of a significant activation energy barrier for dissociation reactions of adsorbed molecules. Further electronic changes such as lowering of the LDOS at the Fermi level, as observed directly with STM [28], and/or structural changes involving the loss of all pure-Pt 3-fold hollow sites, upon forming the $\sqrt{3}$ alloy decrease the reactivity of this alloy even further.

$C_{10}H_{18}$ and $C_{12}H_{22}$ desorb in a single, well-defined, characteristic peak for each of the three surfaces, like that observed previously for cyclohexane and other alkane molecules. Thus, $C_{10}H_{18}$ and $C_{12}H_{22}$ desorb with little sensitivity to the presence of individual Pt and Sn atoms in the surface layer of these Pt–Sn alloys. $C_{10}H_{18}$ and $C_{12}H_{22}$ adsorption energies on Pt(1 1 1) are decreased, but only a small amount, upon alloying with Sn. For example, these energies are lowered by 14% and 6%, respectively, when comparing Pt(1 1 1) to the $\sqrt{3}$ alloy with $\theta_{Sn} = 0.33$. Changes in electronic structure have weak effects on saturated hydrocarbons because they interact with metal surfaces primarily via van der Waals or polarization interactions. In contrast, the ethylene adsorption energy is decreased by 40% comparing Pt(1 1 1) to the $\sqrt{3}$ alloy due to the strong interaction between fully rehybridized, di-σ-bonded ethylene molecules and the Pt(1 1 1) surface [42]. We note that the adsorption energy of $C_{10}H_{18}$ on Pt(1 1 1) decreased upon alloying more than that of $C_{12}H_{22}$. This may be caused by the difference in molecular geometry. The σ bond between the two rings in $C_{12}H_{22}$ allows this molecule slightly greater flexibility in adjusting the adsorption geometry on the alloy surfaces.

Finally, we point out that there is only a small decrease in the $C_{10}H_{18}$ and $C_{12}H_{22}$ monolayer saturation coverage in comparing Pt(1 1 1) with the two Sn/Pt(1 1 1) alloys. This fact should be considered in discussing and modeling catalytic reactions on these alloy surfaces: up to one-third of a

monolayer of alloyed Sn does not effectively block sites for adsorption of such molecules.

5. Conclusions

$C_{10}H_{18}$ (*trans*-decahydronaphthalene) and $C_{12}H_{22}$ (bicyclohexane) are partially reversibly adsorbed on Pt(1 1 1) at 110 K, with some decomposition occuring during TPD. The only gas-phase decomposition product detected was H_2. $C_{10}H_{18}$ desorbs from Pt(1 1 1) at 275 K with a desorption activation energy of $E_d = 70$ kJ/mol, and 13% of the adsorbed monolayer fully dehydrogenates to produce surface carbon during TPD. $C_{12}H_{22}$ desorbs from Pt(1 1 1) at 291 K with $E_d = 75$ kJ/mol, and 25% of the adsorbed monolayer fully dehydrogenates to produce surface carbon during TPD. The presence of alloyed Sn in the surface layer of the two surface alloys, the (2×2)-Sn/Pt(1 1 1) with $\theta_{Sn} = 0.25$ and $(\sqrt{3} \times \sqrt{3})R30°$-Sn/Pt(1 1 1) with $\theta_{Sn} = 0.33$, caused only a small decrease in the monolayer coverages and a relatively small decrease in the adsorption energies of these molecules. $C_{10}H_{18}$ and $C_{12}H_{22}$ desorb at lower temperatures from these Sn/Pt(1 1 1) surface alloys in single, narrow characteristic peaks. $C_{10}H_{18}$ is completely reversibly adsorbed on both of the two Sn/Pt(1 1 1) alloys and no decomposition occurs upon heating in TPD. The decomposition of $C_{12}H_{22}$ during TPD is reduced to 10% of the monolayer on the (2×2) surface alloy and eliminated on the $\sqrt{3}$ surface alloy. In addition to providing additional insight into the chemistry of bicyclic hydrocarbons on Pt and Pt–Sn alloy surfaces, these measurements enable us to improve our estimates of the activation energy barriers for breaking aliphatic C–H bonds in hydrocarbons adsorbed on Pt–Sn alloy surfaces. We find that $E^* = 65$–73 kJ/mol on the (2×2)-Sn/Pt(1 1 1) surface alloy and $E^* > 70$ kJ/mol on the $(\sqrt{3} \times \sqrt{3})R30°$-Sn/Pt(1 1 1) surface alloy.

Acknowledgments

This work was supported by the Department of Energy, Office of Basic Energy Sciences, Chemical Sciences Division.

References

[1] Z. Karpinski, J.K. Clarke, J. Chem. Soc. Faraday Trans. I 71 (1975) 893.
[2] B.H. Davis, J. Catal. 46 (1977) 378.
[3] H. Verbeek, W.M.H. Sachtler, J. Catal. 42 (1976) 257.
[4] R.D. Cortright, J.A. Dumestic, Appl. Catal. A 129 (1995) 101.
[5] R.D. Cortright, P.E. Levin, J.A. Dumestic, Ind. Eng. Chem. Res. 37 (1998) 1717.
[6] J.M. Hill, R.D. Cortright, J.A. Dumestic, Appl. Catal. A-Gen. 168 (1998) 9.
[7] D.A. Hickman, L.D. Schmidt, Science 259 (1993) 343.
[8] A.S. Bodke, D.A. Olschki, L.D Schmidt, Science 285 (1999) 712.
[9] L.S. Liebmann, L.D Schmidt, Appl. Catal. A-Gen. 179 (1999) 93.
[10] V. Ponec, G.C. Bond, Stud. Surf. Sci. Catal. 95 (1995) 477.
[11] C. Xu, B.E. Koel, M.T. Paffett, Langmuir 10 (1994) 166.
[12] C. Xu, Y. Tsai, B.E. Koel, J. Phys. Chem. 98 (1994) 585.
[13] Y. Tsai, B.E Koel, Langmuir 14 (1998) 1290.
[14] J.W. Peck, D.I. Mahon, B.E. Koel, Surf. Sci. 410 (1998) 200.
[15] J.W. Peck, D.I. Mahon, D.E. Beck, B.E. Koel, Surf. Sci. 410 (1998) 170.
[16] C. Panja, N. Saliba, B.E. Koel, Surf. Sci. 395 (1998) 248.
[17] Y. Tsai, C. Xu, B.E. Koel, Surf. Sci. 385 (1997) 37.
[18] Y. Tsai, B.E. Koel, J. Phys. Chem. B 10 (1997) 2895.
[19] J.W. Peck, B.E. Koel, J. Am. Chem. Soc. 99 (1995) 16670.
[20] C. Xu, B.E. Koel, Surf. Sci. 304 (1994) 249.
[21] E.A. Carter, B.E. Koel, Surf. Sci. 226 (1990) 339.
[22] B.E. Koel, D.A. Blank, E.A Carter, J. Mol. Catal. A: Chem. 131 (1998) 39.
[23] N. White, PCT Int. Appl. (1985) 56.
[24] M.T. Paffett, R.G. Windham, Surf. Sci. 208 (1989) 34.
[25] S.H. Overbury, D.R. Mullins, M.T. Paffett, B.E. Koel, Surf. Sci. 254 (1991) 45.
[26] A. Atrei, U. Bardi, G. Rovida, M. Torrini, E. Zanazzi, P.N. Ross, Phys. Rev. B 46 (1992) 1649.
[27] M. Galeotti, A. Atrei, U. Bardi, G. Rovida, M. Torrini, Surf. Sci. 313 (1994) 349.
[28] M. Batzill, D.E. Beck, B.E. Koel, Surf. Sci. 466 (2000) L821.
[29] J. Kuntze, S. Speller, W. Heiland, A. Atrei, I. Spolveri, U. Bardi, Phys. Rev. B 58 (1998) 24.
[30] H. Zhao, J. Kim, B.E. Koel, Surf. Sci 538 (2003) 147.
[31] R.G. Wndham, M.E. Bartram, B.E. Koel, J. Phys. Chem. 92 (1988) 2862.
[32] K. Christmann, G. Ertl, T. Pignet, Surf. Sci. 54 (1976) 365.
[33] P.A. Redhead, Vacuum 12 (1962) 203.
[34] H. Zhao, B.E. Koel, Surf. Sci., to be submitted.
[35] J.A. Rodriguez, C.T. Campbell, J. Phys. Chem. 93 (1989) 826.
[36] C. Xu, B.E. Koel, M.A. Newton, N.A. Frei, C.T. Campbell, J. Phys. Chem. 99 (1995) 16670.

[37] L.Q. Jiang, A. Avoyan, B.E. Koel, J.L. Falconer, J. Am. Chem. Soc. 115 (1993) 12106.
[38] R.T. Morrison, R.N. Boyd, Organic Chemistry, Allyn and Bacon, Boston, 1973.
[39] M.T. Paffett, S.C. Gebhard, R.G. Windham, B.E. Koel, J. Phys. Chem. 94 (1990) 6831.
[40] Y. Li, M.R. Voss, N. Swami, Y. Tsai, B.E. Koel, Phys. Rev. B 56 (1997) 15982.
[41] S. Pick, Surf. Sci. 436 (1999) 220.
[42] M.T. Paffett, S.C. Gebhard, R.G. Windham, B.E. Koel, Surf. Sci. 223 (1989) 449.